Arch. Metall. Mater. **67** (2022), 1, 203-208

DOI: https://doi.org/10.24425/amm.2022.137490

D. MIGAS[1*], T. LIPTAKOVA[2], G. MOSKAL[1]

EFFECT OF RARE EARTH CERIUM ADDITION ON OXIDATION BEHAVIOR OF Co-Al-W ALLOYS AT 800°C

The γ/γ′ Co-based alloys are a new class of cobalt superalloys, which are characterized by remarkable high temperature strength owing to strengthening by γ′-Co_3(Al, X) phases. In this investigation, the effect of cerium addition on oxidation behavior of model Co-Al-W alloys was studied. The introduction of Ce aimed at improvement of the oxidation resistance of γ′-forming Co-based superalloys. The minor additions of cerium (0.1, 0.5 at.%) were added to the base alloy Co-9Al-9W. The alloys were prepared via induction vacuum melting (VIM). Further, a primary microstructure of the alloys was analyzed with particular regard to a segregation of Ce. The thermogravimetric analysis (TG) under non-isothermal conditions was used to preliminary estimate the oxidation behavior of alloys at different temperatures. During experiment, differential thermal analysis (DTA) was performed simultaneously. After this test, cyclic oxidation expermients was carried out at 800°C for 500 h.

In as-cast state, Ce segregates to interdendritic areas and forms intermetallic phases. The effect connected with melting of interdendritic precipitates was observed at 1160°C. Ce-containing alloys were less prone of oxide spallation. Moreover, oxidation rate of these alloys substantially decreased after 100h of oxidation, whereas mass of the sample corresponding to base alloy continued to increase.

Keywords: rare earth elements; REE; cyclic oxidation; γ-γ′ cobalt-based superalloys; Co-Ce

1. Introduction

Since decades, the γ′-strengthened superalloys are important structural materials. The successful application of Ni-superalloys in aircraft industry was possible owing to remarkable mechanical properties at high temperature. The high temperature strength of alloys is mainly owing to double-phase γ-γ′ microstructure. In this case, the strengthening is provided by precipitation of coherent γ′-Ni_3(Al, Ti) of $L1_2$ type [1]. The new groups of superalloys which have attracted considerable attention over past years are γ-γ′ Co-based superalloys. The γ′-forming Co-based superalloys have been widely studied over last 15 years. The phrase γ′-strengthened Co-based superalloys was introduced in 2006 for the first time by Sato et al [2]. The first system which exhibit γ′-phase was Co-Al-W, which is the most known at the current state. In the system, the following phases were found: γ-Coss, γ′-Co_3(Al, W), β-CoAl, χ-Co_3W, μ [3]. The remarkable mechanical properties of the alloys are achieved owing to precipitation of ternary γ′ phase within γ matrix. The stability of this phase as well as oxidation resistance of the ternary alloys alloys are strongly attributed to W-content [4, 5]. Ni addition may cause γ/γ′ microstructure more stable by increasing solvus temperature [6]. The influence of alloying elements on mechanical properties of Co-Al-W alloys by addition of B , Mo, and Ta was studied [7-12]. A relatively high attention has been paid to B-addition. Despite enhancement of mechanical properties, this element also plays role in improvement of oxidation properties [13-15]. In general, alloys based on Co-Al-W system are not able to form protective oxide scale at high temperatures. The formation of o discontinuous inner alumina layers was observed at 800 and 900°C. However, such oxide layers only provide a localised protection, and hence a barrier to oxygen transport is not satisfactory. B-addition promotes growth of the inner alumina layer after long-time exposure at 800°C, hence may hamper further oxidation at this temperature. An another element which may both improve mechanical and oxidation properties is Ce [16,17]. The improvement of isothermal oxidation resistance via doping Ce was confirmed in the case of Co-Al-W-Mo-Ta-B system at 800°C [17]. The authors varied Ce-content from 0.01 to 0.2 at.%. The oxidation rate decreased as Ce-amount in the alloy increased. Furthermore, other authors [18] found doping with 0.02 at.% rare earth elements improved isothermal oxidation behavior of Co-9Al-10W alloys.

[1] SILESIAN UNIVERSITY OF TECHNOLOGY, FACULTY OF MATERIALS ENGINEERING, DEPARTMENT OF MATERIALS TECHNOLOGIES, KATOWICE, POLAND
[2] UNIVERSITY OF ZILINA, FACULTY OF MECHANICAL ENGINEERING, DEPARTMENT OF MATERIAL ENGINEERING, ZILINA, SLOVAK REPUBLIC

* Coresoponding author: damian.migas@polsl.pl

Addition of cerium in the case of superalloys was studied in the case of Fe and Ni-based superalloys, especially in the case of chromia-forming alloys [19-21]. However, the data concerning effect of this element on high temperature oxidation is limited the case of Cobalt superalloys and alloys which do not form Cr_2O_3. In this study, the influence of cerium on as-cast microstructure and high temperature oxidation was investigated. The study aimed in characterization of primary microstructure, microsegregation and the cerium effect on high temperature exposure of the Co-Al-W alloys. Furthermore, the oxidation behavior of under cyclic conditions in view of oxide spallation was evaluated.

2. Materials and methods

The base Co-9Al-9W (at. %) alloy and its Ce-added modifications (containing 0.1 and 0.5% Ce respectively) alloys were prepared via vacuum induction melting (VIM). The ϕ18 mm ingots were melted using furnace VSG 02 Balzers and casted under Ar atmosphere. Pure Co, Al, W, Ce metals were used in a preparation of the investigated materials. The alloys were melted in the temperature range 1600÷1700°C in a time of approx. 10 min. The investigated alloys were casted into graphite molds, under the Ar protective atmosphere. The alloys were investigated in as-cast state. After casting, metal slices of ~3 mm thickness were cut from the ingot via electrical discharge machining (EDM).

Surfaces of prepared metal specimens were ground, polished, and then cleaned and degreased. The samples were exposed to cyclic oxidation 800°C for 500 hours. The oxidation tests were carried out in a laboratory furnace working in air. One oxidation cycle included oxidation for 25 h, air cooling outside a furnace, and specimen mass measurement using laboratory balance with a resolution of 0:10 mg. The samples were placed in alumina crucibles in order to maintain oxide spallation products. After cooling to room temperature, specimens were weighted with and without crucible. Such measurements allow for determination of intensity of oxide spallation. After 200 h of oxidation, the duration of cycle was elongated from 25 to 50h. The test temperature was selected basing on thermogravimetric analysis (TG). The analysis of as-cast alloys under non-isothermal conditions was performed on NETZSCH STA 449 F3 Jupiter device from 40 to 1200°C. The specimens ~4 × 4 × 10 mm used in the investigation were ground using SiC paper down to 1200 grid and ultrasonically cleaned in acetone. The oxidation of samples contained in Al_2O_3 crucibles was carried out in air at heating rate 5°C min^{-1}. During TG experiment, differential thermal analysis (DTA) was performed simultaneously.

Apart from cyclic oxidation, other samples were isothermally oxidized at 800°C of 100 h in order to evaluate oxide scale. The characterization of oxidation products included microscopic analysis in cross section of a specimen. The analysis of a primary microstructure was performed by means of light microscopy (LM) and scanning electron microscopy (SEM). The LM micrographs were performed using the Nikon Eclipse MA200 microscope. In the case of SEM/EDS analysis, the scanning electron microscope (SEM, Hitachi S-3400N) equipped with the energy dispersion spectrometer (EDS, Thermo Noran System Seven) was used. The specimens for SEM were not etched. However, in order to reveal a dendritic structure by LM observations, a reagent containing 25 mL H_2O, 50 mL HCl, 15 g $FeCl_3$ and 3 g $CuCl_2 \times NH_4Cl_2 \times H_2O$ was used for etching. Moreover, on as-cast specimens, the X-ray diffraction measurements in Bragg-Brentano geometry were done using Panalytical Empyrean X-Ray Diffractometer diffractometer fitted with a copper anode tube ($\lambda_{CuK\alpha}$ – 1.54178 Å), operating at 40 mA/45 kV. Recording was performed with a stepwise approach of 0.02° step in the range of 10 to 90° 2θ.

3. Results and discussion

The investigated alloys were analyzed in view of phase composition. The analysis was performed on specimens cut from a middle part of ingots. The results of X-ray diffraction analysis are shown in Fig. 1. The all detected peaks are corresponding to fcc Co (JCPDS no 15-0806). Although Ce is not expected to dissolve in Co-matrix [22], no peaks corresponding to phases other than Co were found in the case of alloys containing 0.1 and

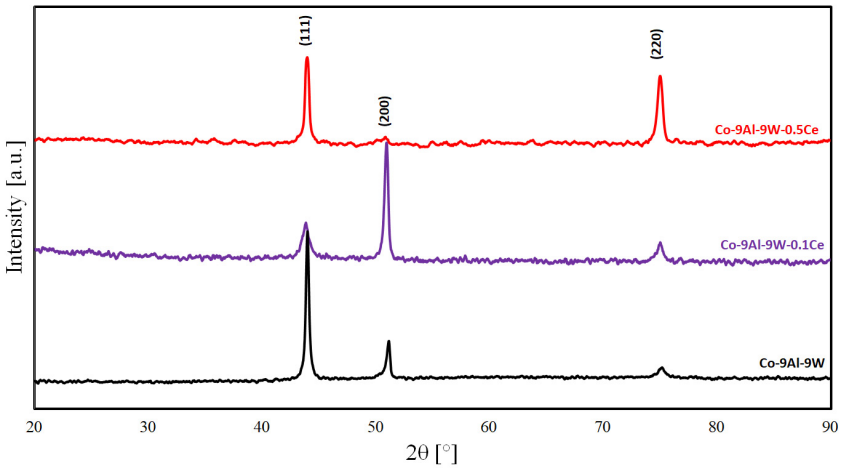

Fig. 1. XRD patterns of investigated alloys in as-cast state

0.5 at.% Ce respectively. In order to observe Ce-segregation, a microscopic analysis was performed.

The microstrcture of Ce-containing alloys is shown in Fig. 2. The LM micrographs (Nomarski contrast) of all three alloys (Fig. 2a-c) show typical dendritic microstructure in all cases. The observations of BSE images indicates segregation of some elements in intedrendritic areas. In the case of base alloy (Fig. 2d), the interdendritic areas are slightly enriched in Al, which was investigated in our study [24]. In the case of Ce-doped alloys (Fig. 2e-f), Al-enrichmend (areas marked by points no. 2 and 5 respectively) occurred as well. In these areas, content of this element was higher compared to that of dendrite cores (Tab. 1), whereas no cerium was detected. Except of Al-enrichment, segregation of Ce (areas marked by points no. 3 and 6 respectively) was noticed in the interdenrtitic spaces. The fraction of interdenritic phases is higher in the case of alloy containing 0.5%Ce. In view of chemical composition in micro areas, except of cerium, the observed zones are enriched in Al similarly to other, Ce-free interdendritic spaces. Furthermore, the observed Ce-rich phases are substantially depleted in W.

In order to show microsegregation of Ce-containing alloys clearer, the energy dispersive spectroscopy elemental mapping images were made (Fig. 3). Such mapping images present qualitatively spatial distributions and local enrichments of the individual elements. The distribution confirmed occurrence of three structural elements: dendrites rich in Co, Al and W ("A"), interdendritic spaces containing only Co, Al and W ("B"), and ternary Ce-Co-Al phases located in the intedendritic region ("C"). Taking into account equlibrium conditions at higher temperatures [23,24], the following ternary phases Ce-Co-Al phases were found: CeCoAl, $CeCoAl_4$, $CeCo_2Al_8$, $Ce_2Co_{15}Al_2$ [23], $Ce_2Co_6Al_{19}$, $Ce_3Co_3Al_4$ [24]. In view of chemical composition, the most probable ternary phase to occur is $Ce_2Co_{15}Al$ or possibly $CeCo_4Al$. The phases which may be expressed as $Ce_2Co_{17-x}Al_x$ and $Ce_{5-x}Al_x$ are extensions from binary Ce_2Co_{17} and $CeCo_5$ phases, which are formed as a results of substitution of Co atoms by Al [25].

TABLE 1

Chemical composition in micro areas marked in Fig. 2, measured by EDS in at.%

Point	Element			
	Al-K	Co-K	Ce-L	W-M
1	4.8	88.4	—	6.8
2	6	87.8	—	6.2
3	6.4	80.1	13.1	0.4
4	5	87.7	—	7.3
5	7.1	80.7	10.9	1.3
6	6.2	87.8	—	6

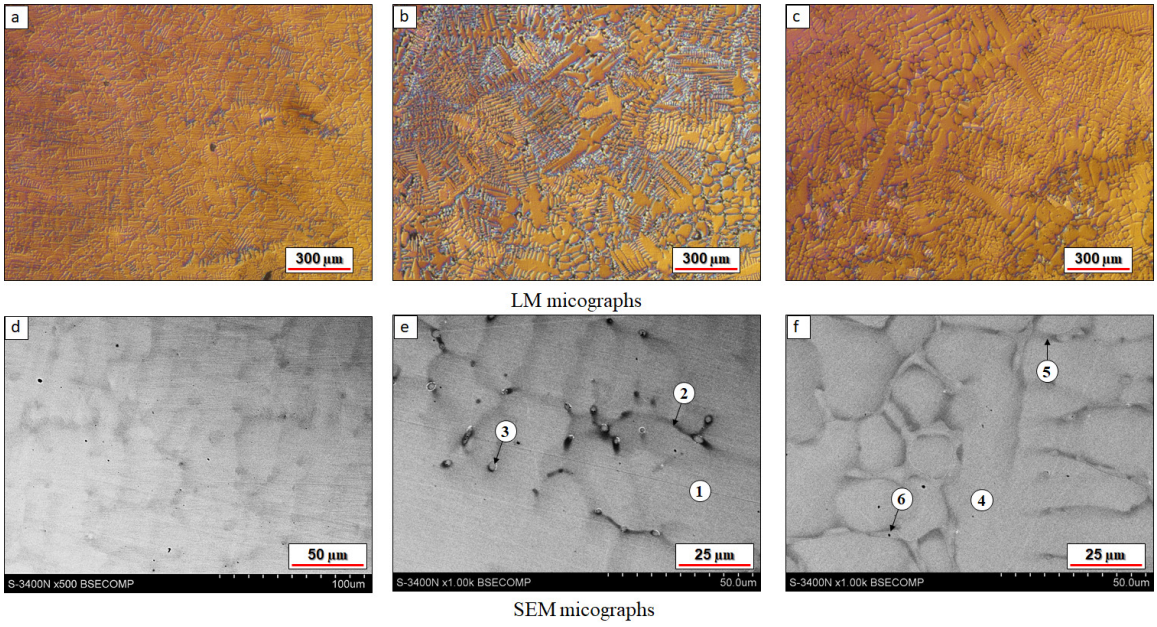

Fig. 2. LM and SEM images of primary microstructure of investigated alloys: a, d) Co-9Al-9W; b, e) Co-9Al-9W-0.1Ce; c, f) Co-9Al-9W-0.5Ce

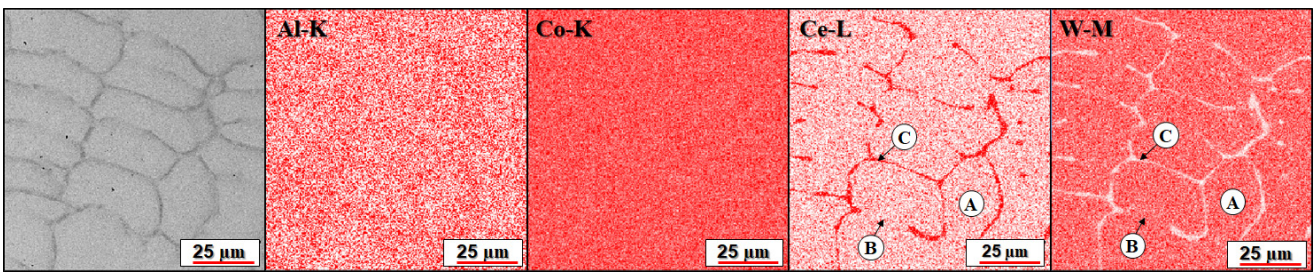

Fig. 3. Qualitative elemental mapping images of Al, Co, Ce, W in as-cast Co-9Al-9W-0.5Ce alloy

The further part of studies concerned TG/DTA analysis of the investigated alloys (Fig. 4). Taking into account the mass gain as a function of temperature, there are no substantial differences caused by Ce-alloying. In view of plot course, oxidation became more intense at above 800°C). Due to character of oxidation above 800°C, and in view of literature data, temperature of further cyclic oxidation test was 800°C. The DTA curves shows occurrence of endothermic peaks below 1000°C ("A"). Taking into account a shape of peak, this thermal effect should be connected with order-disorder transition [26,27]. In this case, the effect is connected with transition of γ′-Co_3(Al, W) to γ phase, which is widely described in the literature data. Another endothermic peaks were recognized at ca. 1160°C ("B"). Taking into account a shape of peak and its derivative (Fig. 4b), the observed thermal effects is characteristic for melting process. The observed peaks, which were not noticed for reference alloy, may correspond to melting of Ce-containing phases. Taking into account binary Co-Ce system [28], the temperature of Ce_2Co_{17} and $CeCo_5$ formation upon cooling is 1210 and 1194°C respectively. Therefore, the observed peaks are believed to be corresponding to a Ce-rich interdendritic phase. Unfortunately, there is no literature data concerning thermal effect concomitant crystallization or melting of phases from Co-Al-Ce system. Therefore, peaks observed in the case of alloys doped with Ce can not be directly attributed to any specific ternary phase basing on the literature data. Some DSC thermograms corresponding to Ce-Co-Al system are available [29,30]. However, the data is corresponding to high-Al parts of this system. In general, Co-rich phases of Ce-Co-Al system are of interest in the case of magnetic materials [25,31], whereas ternary Ce-Co-Al phases have been never found in cast alloys. Taking into account data concerning single phases from Ce-Co-Al system, substitution of Co atoms by Al decrease the curie temperature [25]. Moreover, introduction of Al to Co_{ss} decreases its melting temperature [32]. Taking into consideration that melting of ternary phase may occur at 1160°C, the operating temperature of alloys composed of such phase could not exceed the temperature of its melting, especially under mechanical loads. The heat treatment should result in accumulation of the phase in grain boundaries. Local melting of phase under mechanical load may result in occurrence of a failure. The maximum solubility of Ce in Co is 0.04 at.% (at 1000°C) [28], however, there is no data concerning Ce-solubility in Co in the case of multicomponent systems. Although the solvus temperature of model Co-Al-W alloys is slightly lower than 1000°C, different alloying elements increase this boundary. In the case of newly developed alloys, the order-disorder tranistion may occur at temperatures higher than 1100°C. In the case of alloys considered for operation at temperatures over 1100°C, presence of Ce-rich intermetallics phases may be harmful, especially in the case of phases characterized by partial substitution of Co by Al. Although, W does not form any ternary phases with Co and Ce, recent developed alloys often contain other alloying elements such as Ti, Ta, Mo, Nb, V and other. From this point of view, it would be of interest to evaluate possible formation and the melting temperature of

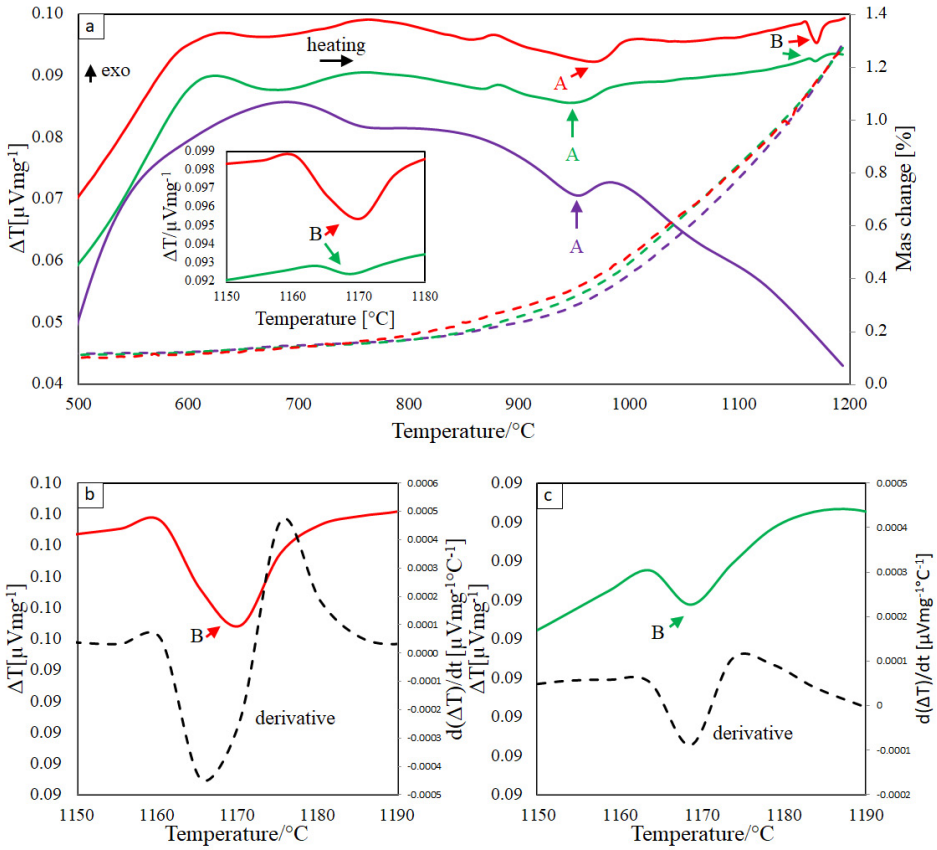

Fig. 4. TG/DTA plots of investigated alloys: a) TG and DTA plots in the temperature range 500-1200°C; b) DTA and DDTA plots of Co-9Al-9W-0.5Ce in the temperature range 1150-1190°C; c) DTA and DDTA plots of Co-9Al-9W-0.1Ce in the temperature range 1150-1190°C

Ce-$Co_{17-x}TM_x$ phases (if exist) or other ternary and quaternary Ce-Co-TM phases of different stoichiometry.

The last part of studies was connected with high temperature cyclic oxidation. Fig. 5. shows the mass gain per unit area, corresponding to cyclic oxidation of the investigated alloys at 800°C. During initial 100h of oxidation, the base alloy exhibited lower mass gain upon oxidation compared to that of Co-9Al-9W-0.1Ce and Co-9Al-9W-0.5Ce alloys. However, the alloy was also characterized by more intense oxide spallation (red bars) in comparison to its Ce-doped analogous alloys. After 25 h of oxidation, ca. 36% of the formed scale peeled off due to cooling. Spallation of oxides was also observed in the case of the alloy containing 0.1%Ce, whereas the intensity of oxide peeling was lower compared to that of reference alloy. Almost no spallation of external layer was observed for alloy with the highest Ce-content. Further 400 h of oxidation did not result in substantial oxide spallation of any alloy. After 100 h of oxidation, mass gain almost stoped in the case of Ce-containing alloys. For alloy containing 0.1%Ce, mass gain after 100 h of oxidation was 7.44 $mgcm^{-2}$ (including oxide spallation after 4th cycle of oxidation), and increased to 7.82 $mgcm^{-2}$ (including oxide spallation after the last cycle of oxidation). The similar observation was made on Co-9Al-9W-0.5Ce alloy, for which the mass gain increase since 4th to the last cycle reached 4.4%, while for the previous alloys the increase was ca. 5%. Such stabilization of oxide scale growth was not observed in the case of Ce-free alloy, for which steady mass gain was observed. Taking into account the final mass increase including oxides which peeled off in all oxidation cycles (a sum of values corresponding to blue and green bars), the highest mass gain was observed in the case of the reference alloy (10.26 $mgcm^{-2}$). The analogous final mass gain for alloys containing 0.1 and 0.5%Ce was 8.01 and 7.58 $mgcm^{-2}$ respectively. The total mass gain of alloy with 0.1%Ce was ca. 22% lower compared to that of reference alloy, whereas Co-9Al-9W-0.5Ce alloy exhibited only ca. 5% lower total mass gain compared to that of alloy characterized by 5 times less Ce-concentration.

The macrograhps corresponding to oxidized samples are shown in Fig. 6. In all cases, an outer oxide layer of gray color may be observed. The most undamaged specimen which was

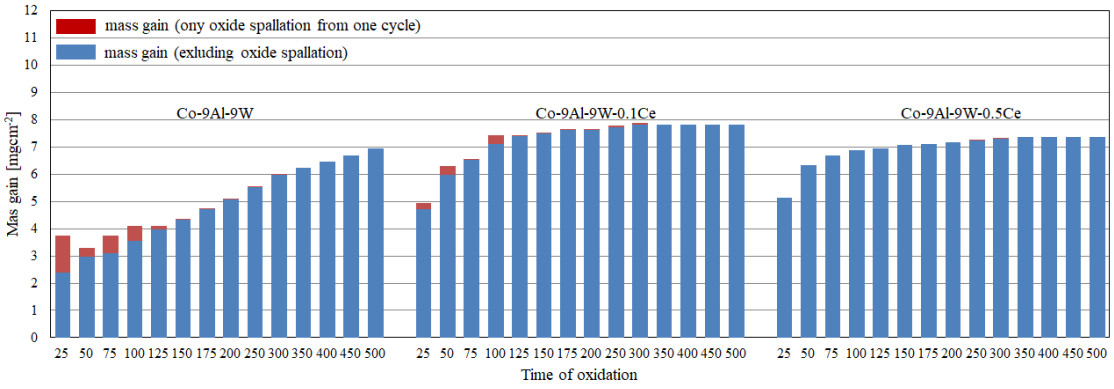

Fig. 5. Mass gain of samples cyclically oxidized at 800°C, related to unit area

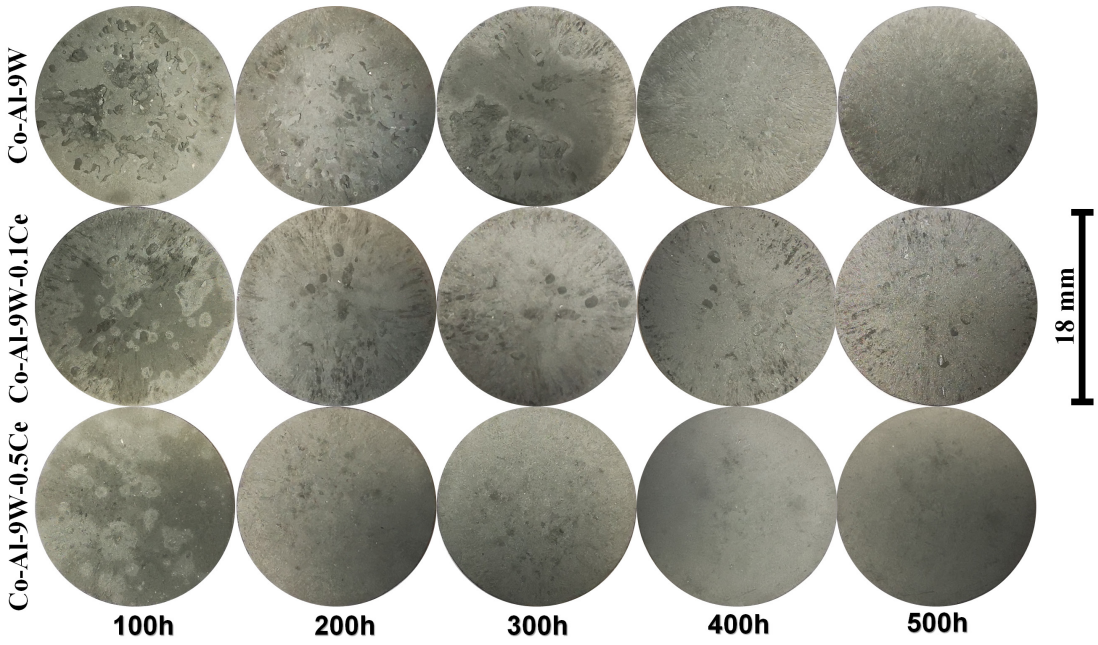

Fig. 6. Macrographs of investigated samples after cyclic oxidation at 800°C

characterized by low oxide spallation was corresponding to Co-9Al-9W-0.5 alloy. More irregular oxidized surface may be observed in the case of other alloys, especially in the case of initial cycles. Due to long exposure time, the characteristic gray layer of single Co-oxides may be observed on the surface of all specimens.

4. Conclusions

The addition of Ce affects the primary microstructure of Co-Al-W alloys via segregation to interdendritic spaces and formation of ternary Ce-Co-Al alloys. In view of Ce-content exceeding solubility of this element in Co, the operating temperature of Ce-doper alloys is limited up to 1160°C due to melting of Ce-rich intermetallic phase. Addition of Ce decreases oxidation rate of Co-Al-W alloys in as-cast state and reduces oxide scale spallation.

Acknowledgments

This work is financed from the budgetary funds for science for the years 2018–2022, as a research project within the Diamond Grant programme (0069/DIA/2018/47).

The authors wish to acknowledge support from The International Visegrad Fund. The research was carried out as part of the Visegrad Scholarship Program, scholarship no. 52010400.

REFERENCES

[1] Y. Wu, C. Li, X. Xia, H. Liang, Q. Qi, Y. Liu, J. Mater. Sci. Technol. **67**, 95-104 (2021)

[2] J. Sato T. Omori, K. Oikawa, I. Ohnuma, R. Kainuma, K. Ishida, Science **312**, 90-91 (2006).

[3] T. Omori, K. Oikawa, J. Satao, I. Ohnuma, U.R. Kattner, R. Kainuma, K. Ishida, Intermetallics **32**, 274-283 (2013).

[4] F. Pyczak, A. Bauer, M. Göken, U. Lorenz, S. Neumeier, M. Oehring, J. Paul, N. Schell, A. Schreyer, A. Stark, F. Symanzik, J. Alloys Compd. **632**, 110-115 (2015).

[5] M. Weiser, S. Virtanen, Oxid. Met. **92**, 541-560 (2019).

[6] H.-Y. Yan, V.A. Vorontsov, D. Dye, Intermetallics **49**, 44-53 (2014).

[7] K. Shinagawa, T. Omori, K. Oikawa, R. Kainuma, K. Ishida, Scr. Mater. **61**, 612-615 (2009).

[8] P.J. Bocchini, C.K. Sudbrack, R.D. Noebe, D.C. Dunand, D.N. Seidman, Mater. Sci. Eng. A, **682**, 260-269 (2017).

[9] M. Kolb, L.P. Freund, L. Fischer, I. Povstugar, S.K. Makineni, B. Gault, D. Raabe, J. Müller, E. Spiecker, S. Neumeier, M Göken, Acta Mater. **145**, 247-254 (2018).

[10] A. Suzuki, T.M. Pollock, Acta Mater. **56**, 1288-1297 (2008).

[11] G. Feng, H. Li, S.S. Li, J B. Sha, Scr. Mater. **67**, 499-502 (2012).

[12] L. Shi, J.J. Yu, C Y. Cui, X.F. Sun, Materials Letters **149**, 58-61 (2015).

[13] L. Klein, A. Bauer, S. Neumeier, M. Göken, S. Virtanen, Corr. Sci. **53**, 2027-2034 (2011).

[14] L. Klein, Y. Shen, M.S. Killian, S. Virtanen, Corr. Sci. **53**, 2713-2720 (2011).

[15] F. Zhong, F. Fan, S. Li, J. Sha, Progress in Natural Science, **26**, 600-612 (2016).

[16] Z. Tao, F. Zhong, Y. Yu, J. Sha, Progress **29**, 416-424 (2019).

[17] F. Zhong, Z-L. Tao, J-B. Sha, Rare Met. (2020).

[18] Q. Wang, Q. Yao, J.-Z. Song, Y. Wang, Y.-H. Zhu, T. Lu, B.-J. Han, J. Mater. Res. **32**, 2117-2126 (2017).

[19] G.M. Ecer, G.H. Meier, The effect of cerium on the oxidation of Ni-50Cr alloys, Oxid. Met. **13**, 159-180 (1979).

[20] X.L. Pan, H.Y. Yu, G.F. Tu, W.R. Sun, Z.Q. Hu, Effect of rare earth metals on solidification behaviour in nickel based superalloy, Mater. Sci. Technol. **28**, 560-564 (2011).

[21] S. Mingzeng, C. Lishan, Z. Yanjun, X. Linlin, J. Rare Earths **30**, 164-169 (2012).

[22] Y. Qingrong, Z. Huaiying, T. Chengying, P. Shunkang, J. Rare Earths **29**, 650-653 (2011).

[23] N. Nasri, J. Gastebois, M. Pasturel, B. Belgacem, I. Péron, F. Gouttefangeas, B. Hassen, O. Tougait, H. Noël, J. Alloys Compd. **628**, 277-281 (2015).

[24] T. Mikuszewski, A. Tomaszewska, G. Moskal, D. Migas, D. Niemiec, Inż. Mat. **5**, 217-223 (2017).

[25] S.J. Hu, X.Z. Wei, D.C. Zeng, X.C. Kou, Z.Y. Liu, E. Bruck, J.C.P. Klaase, F.R. de Boer, K.H.J. Buschow, J. Alloys Compd. **283**, 83-87 (1999).

[26] K. Kobayashi, R. Kainuma, K. Fukamichi, K. Ishida, J. Alloys Compd. **164** (2005)

[27] T. Maciąg, K. Rzyman, R. Przeliorz, Arch. Metall. Mater. **60**, 1871-1876 (2015).

[28] X. Su, W. Zhang, Z. Du, J. Alloys Compd. **267**, 121-127 (1998).

[29] S.A. Uporov, V.A. Bykov, D. Yagodin, J. Alloys Compd. **589**, 421 (2014).

[30] V. Sidorov, P. Svec, D. Janickovic, V. Mikhailova, L. Sonac, J. Magn. Magn. Mater. **395**, 326 (2015).

[31] B.G. Shen, J.Y. Wang, H.W. Zhang, S.Y. Zhang, Z.H. Cheng, B. Liang, W.S. Zhan, J. Appl. Phys. **85**, 4666 (1999).

[32] H. Okamoto, J. Phase Equilibria Diffus. **17**, 367 (1996).